An investigation of low-field magnetoresistance in the double perovskites $Sr_2Fe_{1-x}Zn_xMoO_6$, x = 0, 0.05, 0.15 and 0.25

2006 J. Phys.: Condens. Matter 18 1601

(http://iopscience.iop.org/0953-8984/18/5/013)

INSTITUTE OF PHYSICS PUBLISHING JOURNAL OF PHYSICS: CONDENSED MATTER

J. Phys.: Condens. Matter **18** (2006) 1601–1612 doi:10.1088/0953-8984/18/5/013

An investigation of low-field magnetoresistance in the double perovskites $Sr_2Fe_{1-x}Zn_xMoO_6$, $x = 0$, 0.05, 0.15 and 0.25

Min Feng Lü[1,2], Jing Ping Wang[1], Jian Fen Liu[1], Wei Song[3], Xian Feng Hao[1], De Feng Zhou[1], Xiao Juan Liu[1], Zhi Jian Wu[1] and Jian Meng[1]

[1] Key Laboratory of Rare Earth Chemistry and Physics, Changchun Institute of Applied Chemistry, Chinese Academy of Sciences, Changchun 130022, People's Republic of China
[2] Graduate School of the Chinese Academy of Sciences, Beijing 100049, People's Republic of China
[3] Analysis Centre, Tianjin University, Tianjin 300072, People's Republic of China

E-mail: jmeng@ciac.jl.cn

Received 5 September 2005
Published 17 January 2006
Online at stacks.iop.org/JPhysCM/18/1601

Abstract

The electrical, magnetic and transport properties of Zn doped polycrystalline samples of $Sr_2Fe_{1-x}Zn_xMoO_6$ ($x = 0, 0.05, 0.15$ and 0.25) with the double perovskite structure have been investigated. The subtle replacement of Fe^{3+} ions by Zn^{2+} ions facilitates the formation of a more ordered structure, while further substitution leads to disordered structure because of the presence of a striped phase. Analysis of the x-ray powder diffraction patterns based on Rietveld analysis indicates that the replacement of Fe^{3+} by Zn^{2+} ions favours the formation of Mo^{6+} ions. The spin-glass behaviour can be explained on the basis of the competition between the antiferromagnetic superexchange and the ferromagnetic double-exchange interaction. The low-field magnetoresistance was moderately enhanced at $x = 0.05$, and its origin was found to be the competition between the decrease of the concentration of the itinerant electrons and the weaker antiferromagnetic superexchange in the antiphase boundaries. An almost linear negative magnetoresistance in moderate field has been observed for $x = 0.25$. A possible double-exchange mechanism is proposed for elucidating the observations; it also suggests a coexistence of (Fe^{3+}, Mo^{5+}) and (Zn^{2+}, Mo^{6+}) valence pairs.

1. Introduction

Recently, tunnelling magnetoresistance (TMR) at room temperature in powder samples of the double perovskites $A_2BB'O_6$ (such as the Sr_2FeMoO_6 system) has attracted much

attention because there were predicted, theoretically and experimentally, to be half-metallic properties [1]. Energy band calculations predicted half-metallic behaviour in the Sr_2FeMoO_6 (SFMO) double perovskite, where the electrons were expected to be highly spin polarized at room temperature [2]. The ideal structure of Sr_2FeMoO_6 can be viewed as a regular arrangement of corner-sharing FeO_6 and MoO_6 octahedra, alternating along the three directions of the crystal, with the Sr cation occupying the voids in between the octahedra. In a simple picture, the ferrimagnetic (FM) structure can be described as an ordered array of parallel Fe^{3+} ($S = 5/2$) magnetic moments, antiferromagnetically coupled with Mo^{5+} ($S = 1/2$) spins. According to this model the saturated magnetization (M_s) should be 4 μ_B in this compound. However, most of the experiments show a reduced M_s [3–5]; one should note the influence of antisite disorder at Fe and Mo sites. In the presence of antisite defects (ASDs), some Fe ions interact with neighbouring Fe ions exhibiting antiferromagnetism (AF) and M_s will be decreased.

In the SFMO system, two types of barrier are believed to be responsible for the TMR. The first type is the grain boundary (GB) insulating barriers; many effects have been ascribed to the microstructure, including the grain size [6] and the properties of grain boundaries [7]. The second type is related to intrinsic behaviour—examples include antisite defects [8], A site doping [9] and antiphase boundaries (APB) [10]. However, there has been little study of atomic substitution at the B sites. Technological applications require the low-field magnetoresistance (LFMR) at room temperature to be very sensitive to the applied field. Sarma *et al* [11] suggested that the ordered structure exhibits a sharp low-field response. The larger the difference in size of the B and B′ atoms or the charges of the B and B′ ions, the greater the chance that the compounds will have an ordered structure. Because the radii of Zn^{2+} ions are larger than those of Fe^{3+} ions, the replacement of Fe^{3+} by Zn^{2+} ions may facilitate the formation of ordered structure. The synthesis of pure polycrystalline SFMO samples with a high degree of cationic ordering was required for a longer time and at a high sintering temperature [5]. However, the size of grains increases with increasing sintering time and the MR decreases with increase in the grain size [12]. Therefore, it is worthwhile to learn of ways to control a high degree of Fe/Mo order with decreased sintering temperature or time.

In this paper we attempt to synthesize samples under the same conditions with a view to investigating the magnetotransport properties with different Zn doping concentrations. The LFMR was moderately enhanced in a low magnetic field for low doping content at room temperature. In addition, the magnetic properties and transport mechanism of polycrystalline samples of $Sr_2Fe_{1-x}Zn_xMoO_6$ ($x = 0, 0.05$ and 0.15) are investigated. We believe that this work will be helpful in the development of magnetoelectronic devices.

2. Experimental details

The samples of $Sr_2Fe_{1-x}Zn_xMoO_6$ ($x = 0, 0.05, 0.15$ and 0.25) were fabricated by conventional solid-state reaction. Stoichiometric amounts of analytical grade $SrCO_3$, Fe_2O_3, MoO_3 and ZnO were mixed, ground and pressed into pellets at 350 MPa. The pellets were then calcined in air at 900 °C for 48 h with intermediate grindings. The pellets were finally sintered in a stream of 4% H_2/Ar at 1000 °C for 6.5 h.

The powder x-ray diffraction data was collected at room temperature by a Rigaku D/MAX-2500V diffractometer with Cu Kα radiation (50 kV, 250 mA) and a graphite monochromator. Transport measurements were performed using a Physical Properties Measurement System (Quantum Design Co. Ltd) in the temperature range of 5–300 K. A standard four-probe technique was used. The dc magnetic measurements were carried out between 5 and 350 K by using a commercial Quantum Design (SQUID) magnetometer, cooling the samples at zero

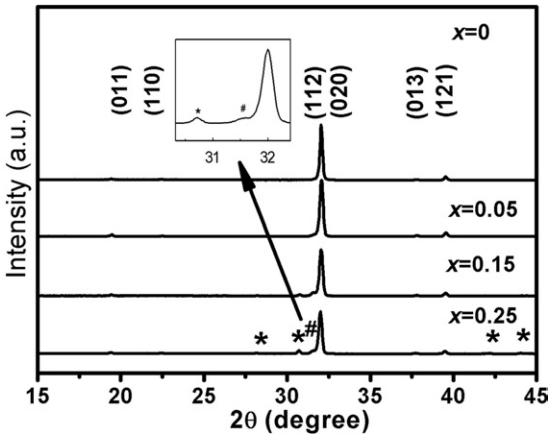

Figure 1. X-ray patterns of polycrystalline $Sr_2Fe_{1-x}Zn_xMoO_6$ ($x = 0, 0.05, 0.15$ and 0.25) samples. The second-phase (Sr_3MoO_6 and striped phase) peaks are separately denoted by $*$ and #.

field and raising the temperature (ZFC curve); field-cooled (FC) dc magnetic susceptibilities were measured with a PPMS system between 5 and 350 K, cooling the samples with an external field and raising the temperature. Both curves were collected with a measuring field of 500 Oe. Magnetization versus applied field curves were measured with a PPMS system at 5 K. Magnetization measurements were also carried out using a Lakeshore VSM-735 with a measuring field of 500 Oe.

3. Results and discussion

3.1. Crystal structure

The XRD patterns of the synthesized samples at room temperature are shown in figure 1. It shows that there are always small amounts of Sr_3MoO_6 and striped phase when $x > 0.10$; the striped phase is comprised of the disordered and deficient phase $SrFe_{1-x-y}Mo_{x-z}O_{3-\delta}$. The undoped sample shows a good quality solid solution, while a small fraction of striped phase was found in the $x = 0.05$ sample within the accuracy of the XRD measurement. In accordance with previous reports [13], Sr_3MoO_6 and the striped phase formed as a result of the evaporation of Fe(O) and Mo(O) after prolonged annealing; at the same time FeO, as well as metallic Fe_2Mo, was also detected. However, these Fe-rich phases are not present in highly doped samples. Because of the difference between the radii and charges of Zn^{2+} ions and Fe^{3+} ions, the replacement of Fe^{3+} ions by Zn^{2+} ions facilitates the formation of the ordered structure. A qualitative estimate of B site ordering is determined by observing the relative intensity of the most intense superstructure reflection. The diffraction intensity ratio $I(011)/[I(020) + I(112)]$ of the Sr_2FeMoO_6 peaks varies from ~0.01 for the $x = 0$ sample and ~0.03 for the $x = 0.05$ sample to ~0.02 for the others. This implies that the slight substitution of Zn^{2+} ions for Fe^{3+} ions ($x = 0.05$) tends to improve the regular arrangement of B and B′ sites in the double-perovskite structure. Both $x = 0$ and 0.05 samples can be indexed in the $I4/m$ space group (No 87), $Z = 2$. Figure 2 illustrates the goodness of fit for the $x = 0$ and 0.05 samples. Table 1 lists the lattice parameters and selected bond lengths of the samples ($x = 0$ and 0.05) determined from analysing x-ray diffraction data using the program GSAS [14]. These x-ray pattern analyses were carried out in two stages. The first was a profile

Table 1. The atomic parameters analysed and selected bond lengths at room temperature for $Sr_2Fe_{1-x}Zn_xMoO_6$ ($x = 0$ and 0.05).

		$x = 0$					$x = 0.05$				
a (Å)		5.570 59(9)					5.571 33(15)				
c (Å)		7.901 55(21)					7.903 01(31)				
Atoms	Positions	x	y	z	Occupancy	U_{iso} (Å^2)	x	y	z	Occupancy	U_{iso} (Å^2)
Sr	4d	1/2	0	1/4	1	0.0213(5)	1/2	0	1/4	1	0.0286(1)
Fe1	2a	0	0	0	0.804	0.0216(8)	0	0	0	0.884(9)	0.0191
Fe2	2b	0	0	1/2	0.196	0.0216(8)	0	0	1/2	0.065(1)	0.0191
Mo1	2b	0	0	1/2	0.804	0.0137(1)	0	0	1/2	0.931(5)	0.0235(5)
Mo2	2a	0	0	0	0.196	0.0137(1)	0	0	0	0.068(5)	0.0235(5)
Zn1							0	0	0	0.046(6)	0.0314(6)
Zn2							0	0	1/2	0.003(4)	0.0314(6)
O1	4e	0	0	0.251(9)	1	0.0488(4)	0	0	0.256(5)	1	0.0338(1)
O2	8h	0.246	0.259(1)	0	1	0.0135(6)	0.244(7)	0.261(3)	0	1	0.0292(7)
Fe1–O1 × 2				1.990					2.027		
Fe1–O2 × 4				1.991					1.995		
Mo1–O1 × 2				1.960					1.924		
Mo2–O1 × 4				1.950					1.947		

matching step, introduced by LeBail [15], with unit cell parameters, profile shape parameters and the individual Bragg intensities varied independently without referring to any structural model. In the second stage, the Rietveld analysis, we have refined the position, the fractional occupancy of the atoms holding the unit cell and the profile shape parameters fixed to the values obtained from the LeBail fit. Refinement of occupancies at B and B′ sites indicates that antisite defects are at 19.6% in the $x = 0$ sample and 11.6% in the $x = 0.05$ sample. A saturation magnetization is evaluated for the simplest ferrimagnetic arrangement (model FIM) [5], which leads to $M_s = (4–8\alpha)\ \mu_B$ (α = ASDs). The results show 2.43 μ_B/f.u. for the $x = 0$ sample and 3.07 μ_B/f.u. for the $x = 0.05$ sample (assuming that the spin contribution of Zn^{2+} ions equals that of Fe^{3+} ions). The average ⟨Fe–O⟩ and ⟨Mo–O⟩ bond lengths of 1.991 and 1.953 Å, respectively, are consistent with those given by Retuerto *et al* [16], 2.003 and 1.947 Å, and, in principle, this apparent difference could account for a more complete B/B′ ordering, since a complete disordering would lead to equal Fe–O and Mo–O distances. The average ⟨Fe–O⟩ and ⟨Mo–O⟩ bond lengths of 2.006 and 1.94 Å, respectively, are in accordance with the rule for the $x = 0.05$ sample.

3.2. Magnetic properties

Figure 3 shows the temperature dependence of the magnetization of the compounds. The samples with $x = 0$ have a lower magnetization which would arise from the disorder of the B and B′ site arrangement [8], which promotes long-range AFM (Fe–O–Fe) superexchange interactions by coupling Fe–O–Mo (AFM) interactions. When the doping ratio is at $x = 0.05$, the magnetization value is the largest; furthermore, for all the samples with their respective doping levels, the magnetization value is higher than that of the undoped one. It can be concluded that all Zn doped samples are sensitive to the applied field. Figure 4 shows the evolution of the temperature of magnetization of the compounds around the Curie temperature (T_c). All curves were normalized at 300 K and shifted up, for clarity. The transition temperature T_c is determined from the extrapolation of the magnetization in the transition

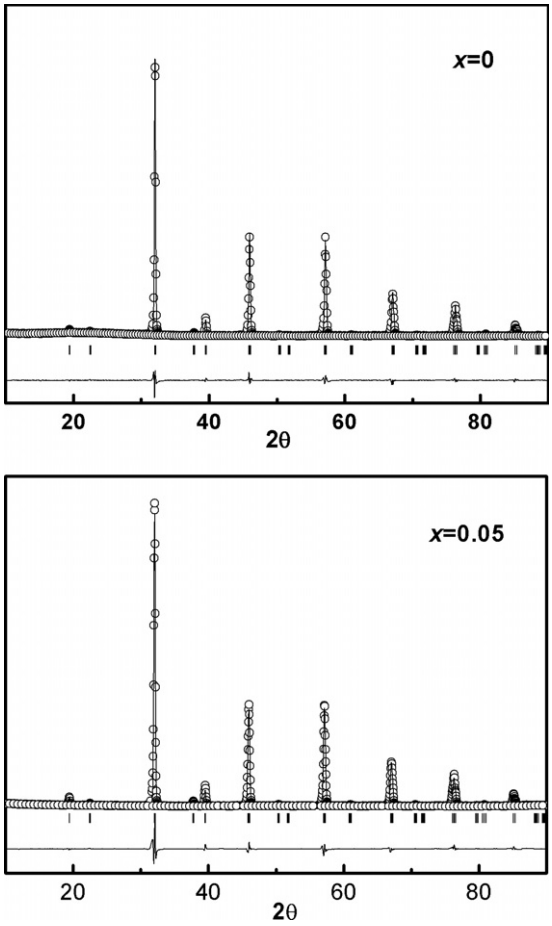

Figure 2. Observed (circles) and calculated (continuous line) x-ray intensity profiles for $Sr_2Fe_{1-x}Zn_xMoO_6$ ($x = 0$ and 0.05). The short vertical lines indicate the angular position of the allowed Bragg reflections. At the bottom in each figure the difference plot, $I_{obs} - I_{calc}$, is shown. The agreement factors for the $x = 0$ sample are $R_{wp} = 10.31\%$; $R_p = 7.13\%$; $R_F = 3.39\%$; and for the $x = 0.05$ sample, $R_{wp} = 11.94\%$; $R_p = 8.31\%$; $R_F = 3.27\%$.

region to zero magnetization. The T_c extracted as a function of Zn content is shown in figure 4 (inset). The measured T_c of every Zn doped sample is higher than that of the pristine one, which is in agreement with our XRD data. The field dependence of the magnetization of $Sr_2Fe_{1-x}Zn_xMoO_6$ samples ($x = 0, 0.05, 0.15$ and 0.25) taken at 5 K is shown in figure 5. The rapid rise of the low-field magnetization of Zn doped samples is magnetically soft. The saturation magnetizations at 5 K for $x = 0, 0.05, 0.15$ and 0.25 are 2.66, 3.08, 2.70 and 2.30 μ_B/f.u. The results for both $x = 0$ and 0.05 samples are consistent with the Rietveld analysis results.

Figure 6 shows the magnetization of the $x = 0.05$ and 0.15 samples registered on warming in a dc field of 500 Oe after cooling in this field (FC) or after cooling without a field (ZFC). The ZFC and FC magnetization measurements support a moderate change in the magnetic character for the Zn doped samples. Both the Zn doped samples show thermomagnetic irreversibilities (differences between the ZFC and FC curves). These features are ascribed to a spin-glass

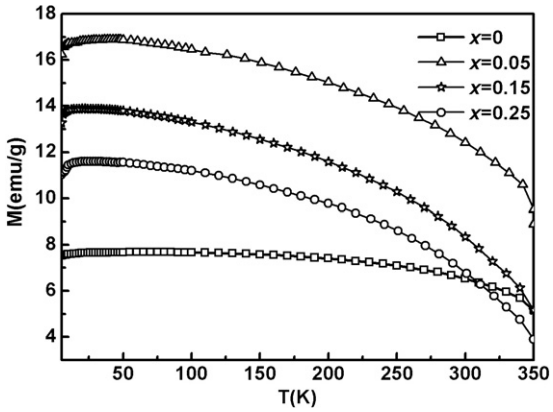

Figure 3. Temperature dependence of the magnetization at 500 Oe.

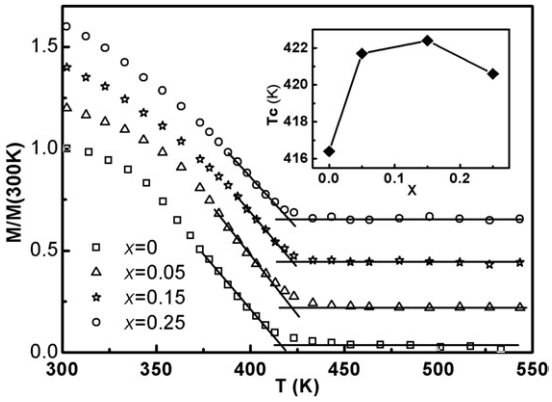

Figure 4. Main panel: temperature dependent magnetization (measured at 500 Oe) for the $Sr_2Fe_{1-x}Zn_xMoO_6$ samples. Curie temperatures were determined from the extrapolation of the transition region (straight lines) to the zero-magnetization level (straight lines). Curves were normalized at 300 K and shifted up in order to clarify the picture. Inset: the evolution of the Curie temperature (T_c) for the $Sr_2Fe_{1-x}Zn_xMoO_6$ series.

behaviour, for further effects, such as magnetic anisotropy, can be discarded, for a relatively small saturation field indicates that the magnetic anisotropy is small. The coercive field drops from 91.06 Oe in the $x = 0.05$ sample to 76.86 Oe in the $x = 0.15$ sample, while the value is 111.48 Oe in the pristine one.

3.3. Magnetotransport measurements

Figure 7 shows the temperature dependence of the MR ($MR = ([\rho(0) - \rho(H)]/\rho(0)) \times 100\%$) in the same magnetic field of 4 kG for all the samples with their respective doping levels. The LFMR ratio for the sample of $x = 0.05$ has a trend, i.e. the MR decreases slowly with increasing temperature. The $x = 0.15$ samples have a stronger temperature dependence than in the case for $x = 0.05$. The value of the MR is higher than that of the pristine one until about 250 K. Beyond $x = 0.15$, the MR value drops heavily; this seems to suggest that the value of the LFMR for the whole temperature range with increasing component of Zn reaches a threshold saturation value at $x = 0.25$. The MR behaviour about $x = 0.25$ will be further discussed later. The data in this work are remarkably different from those for Cu doped polycrystalline

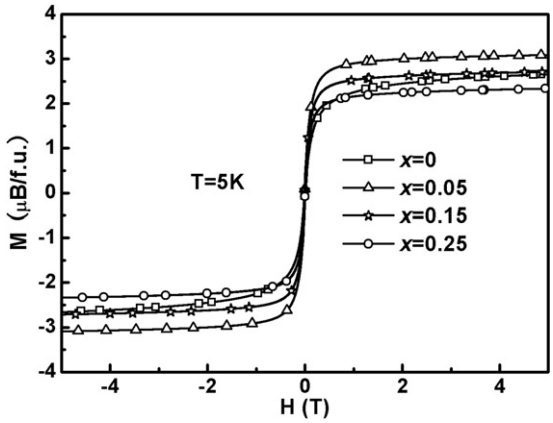

Figure 5. Field dependence of the magnetization of $Sr_2Fe_{1-x}Zn_xMoO_6$ samples ($x = 0$, 0.05, 0.15 and 0.25) at 5 K.

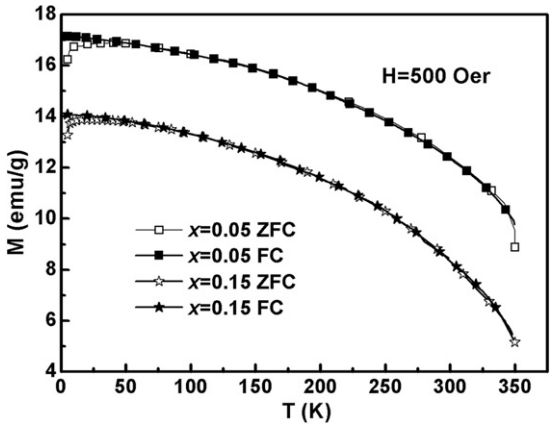

Figure 6. FC and ZFC curves for $Sr_2Fe_{1-x}Zn_xMoO_6$ samples ($x = 0.05$ and 0.15) at 500 Oe.

samples [17]. Comparing with the impurity phase, it can be deduced that the $SrMoO_4$ phase in Cu doped samples grew under light reducing conditions, while Sr_3MoO_6 and the striped phase in this work were present under heavy reducing conditions. However, for all doping level samples, it is impossible to synthesize the pure phase compound under the same reducing conditions.

Figure 8 presents $\rho(H)/\rho(0)$ recorded at various temperatures as a function of the applied field. The value of MR remains almost the same for $H = 5$ T, regardless of the Zn content. In the case of 300 K, a moderate improvement is found on comparing the $x = 0.05$ sample with the pristine one. The LFMR value is the highest for the $x = 0.05$ sample, which is 3.4% at 5 kG at room temperature. In contrast, the $x = 0$ sample exhibits an LFMR of 2.6%. For low Zn contents ($x < 0.25$), the $\rho(H)/\rho(0)$ ratio clearly shows a non-linear tendency in moderate fields, whereas an almost linear MR versus field dependence is observed when $x = 0.25$. This feature was often observed in $Sr_2FeMo_{1-x}W_xO_6$ ($x = 0.2$) below T_c [18], in Ba_2FeMoO_6 [19] around T_c and in $Sr_2FeMn_{1-x}Mo_xO_6$ ($x = 0.05, 0.15$) below T_c [20]. It has been suggested that besides intergrain MR, there exists a large intragrain MR [19]. In the series of W-substituted SFMO, the antiferromagnetic ordering is believed to concentrate in areas where the Fe atoms are surrounded by zero-spin W^{6+} neighbours, while the ferromagnetic order arises from the antiferromagnetic coupling between adjacent Mo and Fe spins [21]. Like W^{6+}, Zn^{2+} may induce zero-spin Mo^{6+}, in the neighbourhood, where the Fe^{2+} ion is in the high-spin state

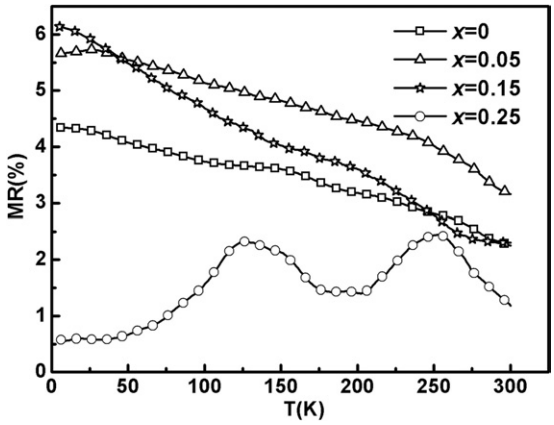

Figure 7. Temperature dependence of the magnetoresistance ratio MR $= [\rho(0) - \rho(H)]/\rho(0)$ for polycrystalline $Sr_2Fe_{1-x}Zn_xMoO_6$ ($x = 0$, 0.05, 0.15 and 0.25) samples at 4 kG.

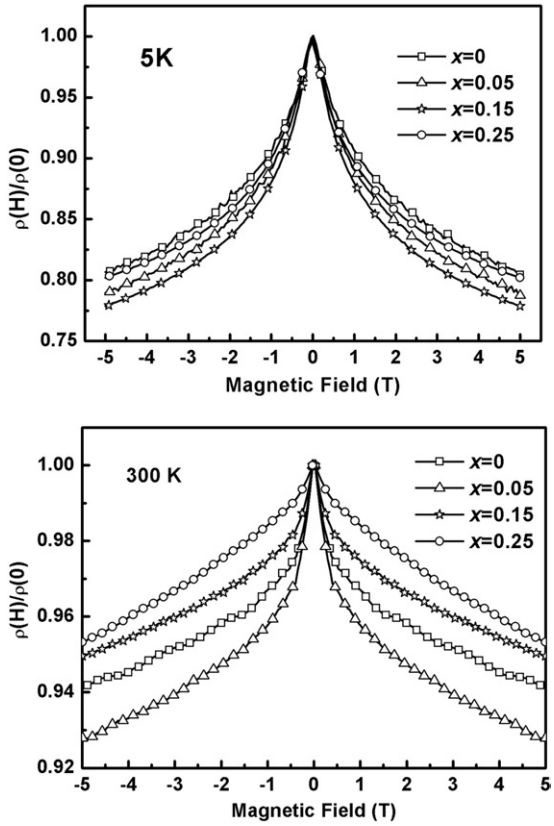

Figure 8. $\rho(H)/\rho(0)$ versus applied external field for the $Sr_2Fe_{1-x}Zn_xMoO_6$ samples at 5 and 300 K.

($s = 2$). The heavily substituted sample ($x = 0.25$) exhibits almost no tunnelling-type MR effect, but still a rather large CMR behaviour. This is an intrinsic effect, which may increase strongly throughout the range of moderate field, particularly in the case of 300 K.

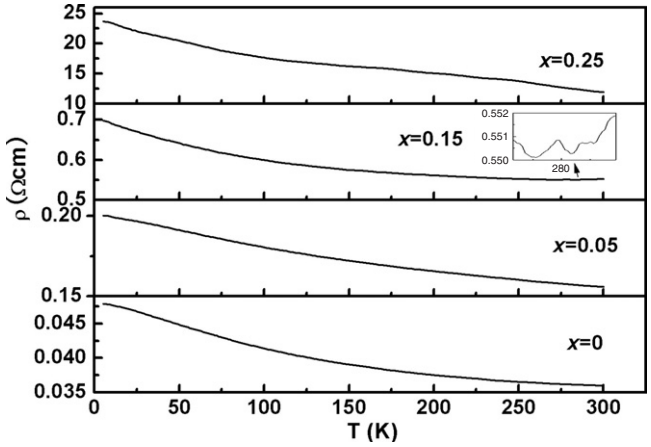

Figure 9. The temperature dependence of the resistivity of samples in zero field for the doping levels $x = 0, 0.05, 0.10, 0.15$ and 0.25.

3.4. Electrical transport properties

Figure 9 shows the temperature dependence of the resistivity for samples ($x = 0, 0.05, 0.15$ and 0.25) in zero field. The pristine one exhibits semiconductor behaviour over the entire measurement temperature region from 5 to 300 K. The resistivity value of the undoped sample ($x = 0$) is close to that of the samples prepared by solid-state reaction at 1200 °C [1]. The samples with higher x have a higher residual resistivity. For samples with low doping content ($x < 0.15$), the resistivity decreases as the temperature increases. For the $x = 0.15$ sample, the resistivity decreases with increasing temperature until a minimum resistivity is reached at about 270 K; after that it increases as the temperature increases further. This temperature transition is also observed for the $x = 0.25$ sample, which exhibits a semiconducting behaviour below 120 K and a resistivity bulking around 180 K under zero field. The resistivity bulking below T_c is frequently observed in colossally magnetoresistive perovskite manganites and could result from a contribution of the non-conductive domain or grain boundary scattering [22]. The data shown in figure 9 may indicate that the contribution of the non-conductive domain is significant for the $x = 0.15$ and 0.25 samples, for there is always a small amount of Sr_3MoO_6. When $x = 0.25$, the resistivity jumps by one order of magnitude. This suggests that there is a percolation mechanism for the transport properties as previously reported. Beyond a critical $x_c = 0.25$ content of the doping element, the volume of the ferromagnetic phase will tend to decrease and the metallicity is suppressed. It should be pointed out that for the $Ba_2Fe_{1-x}Zn_xMoO_6$ compounds, this value is $x_c = 0.40$ [23]. However, Yuan *et al* [17] found that x_c lay somewhere between 0.15 and 0.20 for the bulk $Sr_2Fe_{1-x}Cu_xMoO_6$ samples. This change can be attributed to the difference in the structure parameters of the pristine sample and that of the sizes of the doping ions.

Figure 10 shows the fitting of the variable range hopping model for the samples with different doping concentrations. In the high-temperature range, the resistivity appears to be best described by the variable range hopping (VRH) mechanism $\rho(T) = \rho_0 \exp[(T_0/T)^{1/4}]$, where T_0 is a characteristic temperature. The evaluated values of the parameter T_0 have been listed in table 2. The value of the parameter T_0 decreases from 14.25 for the $x = 0$ sample to 9.96 for the $x = 0.05$ sample and to 5.52 for the $x = 0.15$ sample. These results indicated that the effect of APB inside the grains weakened for Zn doped samples [24].

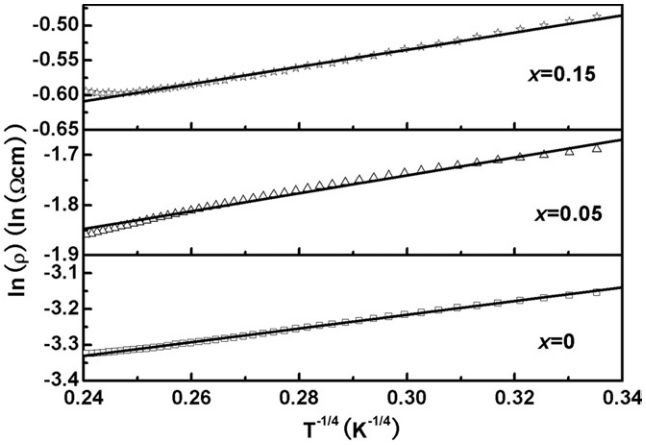

Figure 10. The resistivity as a function of temperature showing that the best fit was the VRH model; —, the linear dependence of $\ln \rho$ on $1/T^{1/4}$ for the samples of $Sr_2Fe_{1-x}Zn_xMoO_6$ ($x = 0, 0.05, 0.15$).

Table 2. The evaluated values of the parameters T_0 and ρ_0 in the linear dependence of $\ln \rho$ on $1/T^{1/4}$ for the samples of $Sr_2Fe_{1-x}Zn_xMoO_6$.

	0	0.05	0.15
T_0	14.28	9.96	5.52
ρ_0	0.023	0.103	0.389
Range (K)	100–300	100–300	100–280

3.5. Discussion

By collectively analysing the experimental results, a reason can be proposed for the influence of Fe site replacement by Zn upon electrical, magnetic and transport properties of polycrystalline samples, especially for the $x = 0.05$ sample. The ZFC and FC curves reflect the existence of magnetic frustration in Zn doped samples. At this point, it may be useful to recall that the simplest superexchange coupling scenario [5], randomly misplaced Fe^{3+} ions at B sites and vice versa, is not expected to induce a substantial magnetic frustration. In this situation, spin-glass-like behaviour is believed to require spin–spin interactions of both ferromagnetic and antiferromagnetic signs which are sufficiently disordered to frustrate ordering systems. As a result, the spin glass in a fully ordered system can occur only in a doping system. We recall that XRD patterns and magnetization data confirm that all samples have ASDs of a certain concentration. Recent measurements of the differential susceptibility have suggested that the existence of some ASDs induced magnetic frustration [25]. At this point, the tendencies of chemical bonding at B′ sites should be described since the substitution at B sites makes direct comparison difficult. In the valence bond model [26, 27], derived from Pauling's rules, the empirical correlation of equation (1) is used to determine the bond valence, S_{ij},

$$S_{ij} = \exp\left(\frac{R_0 - R_{ij}}{B}\right). \tag{1}$$

R_{ij} a chemical bond length, where $B = 0.37$, and R_0 is the length of a bond of unit valence. The value of R_0 used is the bond length of Mo^{5+}.

In practice, equation (1) will be obeyed exactly in an ordered system. But for a partially ordered system, it is not convenient to measure terms for comparison. In order to calculate S_{ij}, it is necessary to sum the bond values at B and B′ sites. A more explicit expression (2) for S_{ij} is

$$S_{ij} = \sum_{ij} \alpha_{ij} S_{ij}(\alpha) \tag{2}$$

where $S_{ij}(\alpha)$ is the chemical bond at B and B′ sites and α_{ij} is the occupation of ions. For the $x = 0.05$ sample, the value of S_{ij} is 5.44, which is higher than that of the $x = 0$ sample ($S_{ij} = 5.2$), indicating that Zn^{2+} ions induce the formation of Mo^{6+} ions. In such a case, the carrier density according to the concentration of the itinerant t_{2g} Mo electrons would be reduced, resulting in the resistivity increasing with increasing doping level. The results are in good agreement with our resistivity data. Moreover, a sort of double-exchange (DE) mechanism is proposed by Zener [28] and Garcia-Landa [29], involving $Fe^{3+} + Mo^{5+} = Fe^{2+} + Mo^{6+}$. This means that the Zn doped system consists of a mixture of antiferromagnetic superexchange and ferromagnetic double-exchange interactions. The observed spin-glass behaviour can be explained on the basis of the competition between these two interactions.

It has been suggested that the APB in double perovskites should be a common defect that may act as strongly pinned magnetic domain walls [30]. In that case one should also expect the saturation to become harder in the presence of APB. After considering the transformation of APB, the LFMR observed in this work will be explained, in that the replacement of Fe^{3+} by Zn^{2+} ions weakens the antiferromagnetic exchange in the APB. The resistivity fitting data have also suggested that the effect of APB was weakened after the replacement of Fe^{3+} ions by Zn^{2+} ions. For the undoped SFMO sample, the APB segregation was produced due to the cationic disorder of the sample. The two segregations nearest to the APB are assumed to have small cationic disorder and therefore the Mo and Fe ions are coupled ferrimagnetically. It is then suggested that these ferrimagnetic order segregations coupled antiferromagnetically across the APB [31]. The antiferromagnetic coupling will become weaker after the Zn replaces the Fe in the APB. The spin in APB will rotate with the external field more easily and thus the MR will be greatly enhanced. However, for Zn doped SFMO ($x < 0.25$) we failed to observe the values of MR increasing rapidly as the value of x increased at 5 K; comparing with the Al doping system [31], this can be explained by the competition between the decrease of concentration of the itinerant electrons and diminished antiferromagnetic superexchange in the APB: on the one hand, the occurrence of Mo^{6+} reduces the degree of spin polarization of Fermi level electrons for these doping samples, resulting in the reduction of the spin-polarized TMR; on the other hand, weakened antiferromagnetic superexchange in the APB makes the spin rotate more easily. In the Zn doping system ($x < 0.25$), the antiferromagnetic superexchange induced by the spin-glass behaviour is more difficult to perturb than the Al nonmagnetic interactions; at the same time, the concentration of the itinerant electrons decreased as the Zn doping increased, and both factors contribute towards the nearly unchangeable MR, comparing with the Al doping system at 5 K. Weakened antiferromagnetic coupling in APB supported the experimental evidence of a smaller enhancement of the MR in the $x = 0.05$ sample around room temperature, although the concentration of itinerant electrons decreased as the Zn doping increased.

A larger temperature dependence of MR in the Zn doped samples of $x = 0.05$ and 0.15 than the case of $x = 0$ occurred; this showed that the role of Zn is also to break the ferromagnetic segregation into smaller ones. This is supported by the residual resistivity of the samples at zero field increasing as the doping Zn increases. As the segregation becomes smaller, it will become more agile under the thermal agitation. As mentioned before, Zn^{2+} ions induce ferromagnetic double exchange and the AFM coupling will become weaker. The spin

in APB will rotate with the external field more easily. In fact, the spin in APB would be more agile under thermal agitation, particularly around room temperature.

However, when the concentration of itinerant electrons decreased further, the effect of the DE mechanism became stronger. In fact, an almost linear MR versus moderate field dependence is an additional indication of the presence of two different MR mechanisms. The investigation of Ba_2FeMoO_6 has shown that, besides the intergrain TMR, there exists a large intragrain MR, which appears near T_c [19]. The large difference in T_c between Ba_2FeMoO_6 and the $x = 0.25$ sample may be explained by the effect of structure, for bulk $Sr_2Fe_{1-x}Cu_xMoO_6$ samples have been observed with high T_c.

Acknowledgment

We offer grateful thanks for the financial support of the National Natural Science Foundation of China (20271049, 20331030).

References

[1] Kobayashi K-I, Kimura T, Sawada H, Terakura K and Tokura Y 1998 *Nature* **395** 667
[2] Sarma D D, Mahadevan P, Saha-Dasgupta T, Ray S and Kumar A 2000 *Phys. Rev. Lett.* **85** 2549
[3] Niebieskikwiat D, Sánchez R D, Caneiro A, Morales L, Vásquez-Mansilla M, Rivadulla F and Hueso L E 2000 *Phys. Rev.* B **62** 3340
[4] Tomioka Y, Okuda T, Okimoto Y, Kumai R, Kobayashi K-I and Tokura Y 2000 *Phys. Rev.* B **61** 422
[5] Balcells Ll, Navarro J, Bibes M, Roig A, Martínez B and Fontcuberta J 2001 *Appl. Phys. Lett.* **78** 781
[6] Yuan C L, Wang S G, Song W H, Yu T, Dai J M, Ye S L and Sun Y P 1999 *Appl. Phys. Lett.* **75** 3853
[7] Niebieskikwiat D, Caneiro A, Sánchez R D and Fontcuberta J 2001 *Phys. Rev.* B **64** 180406
[8] Sánchez D, Alonso J A, García-Hernández M, Martínez-Lope M J, Martínez J L and Anders M 2002 *Phys. Rev.* B **65** 104426
[9] Kim B-G, Hor Y-S and Cheong S-W 2001 *Appl. Phys. Lett.* **79** 388
[10] Goodenough J B and Dass R I 2000 *Int. J. Inorg. Mater.* **2** 3
[11] Sarma D D, Sampathkumaran E V, Ray S, Nagarajan R, Majumdar S, Kumar A, Nalini G and Row T N G 2000 *Solid State Commun.* **114** 465
[12] Han H, Han B J, Park J S, Lee B W, Kim S J and Kim C S 2001 *J. Appl. Phys.* **89** 7687
[13] Liao X Z, Sharma A, Wei M, MacManus-Driscoll J L, Branford W, Cohen L F, Bugoslavsky Y, Zhu Y T, Peterson D E, Jiang Y B and Xu H F 2004 *J. Appl. Phys.* **96** 7747
[14] Larson A C and von Dreele R B 1994 *GSAS: General Structure Analysis System; ANSCE, MS-H805* (Los Alamos, NM: Los Alamos National Laboratory)
[15] LeBail A, Duroy H and Fourquet J L 1988 *Mater. Res. Bull.* **23** 447
[16] Retuerto M, Alonso J A, Martínez-Lope M J, Martínez J L and García-Hernández M 2004 *Appl. Phys. Lett.* **85** 266
[17] Yuan C L, Zhu Y and Ong P P 2004 *J. Appl. Phys.* **91** 4421
[18] Lindén J, Yamamoto T, Nakamura J, Karppinen M and Yamauchic H 2001 *Appl. Phys. Lett.* **78** 2736
[19] Maignan A, Raveau B, Martin C and Hervieu M 1999 *J. Solid State Chem.* **144** 244
[20] Feng X M, Rao G H, Liu G Y, Yang H F, Liu W F, Ouyang Z W, Yang L T, Liu Z X, Yu R C, Jin C Q and Liang J K 2002 *J. Phys.: Condens. Matter* **14** 12503
[21] Kobayashi K-I, Okuda T, Tomioka Y, Kimura T and Tokura Y 2004 *J. Magn. Magn. Mater.* **218** 17
[22] Rao G H, Sun J R, Liang J K and Zhou W Y 1997 *Phys. Rev.* B **55** 3742
[23] Sriti F, Maignan A, Martin C and Raveau B 2001 *Chem. Mater.* **13** 1746
[24] Fang T-T 2005 *Phys. Rev.* B **71** 064401
[25] Navarro J, Balcells Ll, Sandiumenge F, Bibes M, Roig A, Martínez B and Fontcuberta J 2001 *J. Phys.: Condens. Matter* **13** 8481
[26] Brown I D 1992 *Acta Crystallogr.* B **48** 553
[27] Sanches-Salinas A, García-Munoz J L, Rodriguez-Carvajal J, Saez-Puche R and Martinez J L 1992 *J. Solid State Chem.* **100** 201
[28] Zener C 1951 *Phys. Rev.* **82** 403
[29] García-Landa B, Ritter C, Ibarra M R, Blasco J, Algarabel P A, Mahendiran R and García J 1999 *Solid State Commun.* **110** 435
[30] Yin H Q, Zhou J-S, Zhou J-P, Dass R, McDevitt J T and Goodenough J B 1999 *Appl. Phys. Lett.* **75** 2812
[31] Sui Y, Wang X J, Qian Z N, Cheng J G, Liu Z G, Miao J P, Li Y, Su W H and Ong C K 2004 *Appl. Phys. Lett.* **85** 269